ACADEMIC PRESS

Available online at www.sciencedirect.com

SCIENCE DIRECT®

VIROLOGY

Virology 317 (2003) 308–320

www.elsevier.com/locate/yviro

Formation of P10 tubular structures during AcMNPV infection depends on the integrity of host-cell microtubules

Alexandra L. Patmanidi,[a] Robert D. Possee,[b] and Linda A. King[a,*]

[a] *School of Biological and Molecular Sciences, Oxford Brookes University, Gipsy Lane Campus, Oxford, OX3 OBP, UK*
[b] *NERC, Institute of Virology and Environmental Microbiology (CEH), Mansfield Road, Oxford, OX1 3SR, UK*

Received 16 May 2003; returned to author for revision 1 July 2003; accepted 26 August 2003

Abstract

During infection of insect cells with *Autographa californica* nucleopolyhedrovirus (AcMNPV), the very late protein P10 forms large fibrillar structures in the cytoplasm and nuclei of infected cells. In this study we have used confocal microscopy in association with a novel P10 antiserum to localise and study P10 in virus-infected cells. P10 was shown to be a component of tubular-like structures that spiralled throughout the cytoplasm and nucleus of AcMNPV-infected cells. These structures were observed to colocalise partly with cortical microtubules. When microtubules were depolymerised with the drug nocodazole, P10 tubules failed to form and the protein appeared concentrated in cytoplasmic foci. For the first time, we provide direct evidence using both antibody pulldown and yeast two-hybrid experiments for the interaction of P10 with host-cell tubulin. It is suggested that this interaction may be a critical factor in AcMNPV-induced cell lysis.

Keywords: Baculovirus; P10, Cytoskeleton; Actin; Microtubules; Nocodazole; Microtubule-associated proteins; Cell lysis

Introduction

Many baculoviruses, mainly nucleopolyhedroviruses (NPVs), encode a small, very late gene product known as *p10* (Kuzio et al., 1984; Ayres et al., 1994; van Oers et al., 1999; Fielding and Davison, 2000; Razuck et al., 2002). The *p10* gene from *Autographa californica* nucleopolyhedrovirus (AcMNPV), the prototype baculovirus, encodes a protein with a predicted molecular mass of approximately 10 kDa (Ayres et al., 1994). It is synthesised in high levels and forms fibrillar structures in the nucleus and the cytoplasm of AcMNPV-infected cells (Croizier et al., 1987; Quant-Russell et al., 1987; van der Wilk et al., 1987; van Oers et al., 1994). To date, P10 has not been assigned a precise function.

Previous analyses of the amino acid sequence of AcMNPV P10 revealed a coiled-coil domain at the N-terminus of the protein (van Oers et al., 1994; Wilson et al., 1995; van Oers and Vlak, 1997). This part on P10 was shown to be responsible for the self-aggregation of P10 monomers in AcMNPV-infected cells (van Oers et al., 1994; Alaoui-Ismaili and Richardson, 1996). Adjacent to the coiled-coil domain, a proline-rich region has also been identified. This region is conserved among the P10 proteins yet its function is not clear. The carboxy-terminus of P10 consists of basic amino acids and is thought to be involved in the formation of fibrillar structures. The lysine-rich domain on this sequence was initially thought to be a nuclear localisation signal, as it was similar to that identified in polyhedrin (Jarvis et al., 1991); however, P10 partial deletion mutants lacking this basic sequence could still be localised in the nucleus of infected cells (van Oers et al., 1994). The sequence between the proline- rich domain and the basic carboxy-terminus of P10 is highly variable among the P10 proteins (van Oers and Vlak, 1997).

The function of P10 is not known, although it has been suggested that it may be required for the integrity of occlusion bodies, as well as in AcMNPV-induced cell lysis. In virus-infected cells structures called electron-dense spacers

* Corresponding author. Fax: +44-1865-483242.
E-mail address: laking@brookes.ac.uk (L.A. King).

0042-6822/$ – see front matter © 2003 Elsevier Inc. All rights reserved.
doi:10.1016/j.virol.2003.08.035

have also been associated with P10. These structures are often observed to surround the polyhedra and this observation led to the suggestion that P10 may be involved in the proper formation of polyhedra (Williams et al., 1989). The same study demonstrated that insertion/deletion P10 mutant viruses produced loose polyhedron envelopes, which made the occlusion bodies labile under physical stress. More significantly, cells infected with some of these viruses failed to lyse, which led to the second suggestion on the function of P10 as an inducer of cell lysis.

In an earlier study, a monoclonal antiserum raised against the P10 protein from *Orgyia pseudotsugata* nucleopolyhedrovirus (OpMNPV) was shown to recognise cytoskeletal elements, which were subsequently identified as microtubules, suggesting a relationship between the two (Quant-Russell et al., 1987). More recently, the work by Cheley et al. (1992) provided evidence that artificially phosphorylated P10 has microtubule-associated protein (MAP) properties. However, no study to date has established a direct relationship between the P10 and host-cell microtubules, or discovered how such a relationship may contribute to the putative functions of P10.

In this study our aims were to examine the previously predicted relationship between P10 and components of the host cell cytoskeleton, specifically microtubules, using confocal laser scanning microscopy (CLSM) together with a novel anti-P10 specific antiserum. These experiments indicated a close association between P10 and microtubules. This relationship was further investigated by immunoprecipitation and yeast two-hybrid analyses to provide the first direct evidence that the P10 protein from AcMNPV is a virus-encoded microtubule-associated protein. We suggest that this interaction between P10 and microtubules may be involved in a cytoskeleton-induced cell lysis and nuclear disintegration.

Results

Specificity of the novel antiserum for the P10 protein from AcMNPV

To test the specificity of the new antiserum for the P10 protein from AcMNPV, protein samples were analysed using Western blots. Protein extracts from noninfected, mock-infected, AcMNPV-infected (12–72 hpi), or AcΔ*p10*-infected (48 hpi) cells were separated on SDS–polyacrylamide gels (Fig. 1a). The AcΔ*p10* virus, lacking the entire *p10* coding region, was constructed (Fig. 1b) as a negative control for the antiserum. Protein gels were stained with Coomassie Brilliant blue or they were used for protein transfer onto a nitrocellulose membrane (Fig. 1a). On the Western blot, P10 protein was only detected in the lanes corresponding to the samples from AcMNPV, but not in the AcΔ*p10* sample. The bands were specific for P10 and no cross-reactivity was observed with other virus- or host-related proteins.

Immunodetection of P10 in virus-infected cells

The specificity of the P10 antiserum was tested in noninfected and AcMNPV-infected Sf9 cells (24–72 hpi). AcΔ*p10*-infected cells at 72 hpi were also treated with the P10 antiserum and provided a negative control. After staining with the primary antiserum, the samples were labelled with a FITC-conjugated secondary antiserum. In noninfected cells there was no staining with the P10 antiserum, and background fluorescence was minimal (Fig. 2a). By 24 hpi, P10 fibrillar structures began to form in the cytoplasm of AcMNPV-infected cells (Fig. 2b). At 48 hpi, a thick sheath of P10 was observed just inside the plasma membrane and a matrix of P10 was formed in the nucleus (Fig. 2c). This was observed in approximately 70–80% of the infected cells, according to the plane the image was obtained from. Nuclear staining was defined by propidium iodide staining (data not shown). At 72 hpi, the cytoplasmic sheath of P10 had become fragmented, particularly in regions where there were signs of plasma membrane disruption (arrowed, Fig. 2d). Examination of the AcΔ*p10*-infected cells showed that, as expected, P10 was not detected in these cells; however, counterstaining with propidium iodide outlined polyhedra in the infected nuclei (Fig. 2e).

Three-dimensional reconstructions of AcMNPV-infected cells

To examine the distribution of the P10 structures inside whole cells, 3D reconstructions of AcMNPV-infected cells were made. Infected cells at 48 hpi were visualised with confocal microscopy (Fig. 3). Optical sectioning of these cells was carried out to create a Z-stack. Initially, it seemed that these structures were solid, ribbon-like formations, as seen in a stereo projection (Fig. 3a). Closer observations using 3D projections revealed that P10 was forming tubules and their spatial distribution in virus-infected cells was consistent in all the cells examined (Fig. 3b).

To eliminate the possibility of immunostaining artifacts, the P10 tubular structures were examined by optical sectioning (Fig. 3c). Using the principle of data collection for Z-stacks, serial images spanning the cell were collected. An image (*z*-axis) from the medial part of the cell was used as the reference point for optical sections along the two perpendicular axes (*x*- and *y*-). The distribution of the fluorescence from these structures in each individual plane provided evidence of a tubule morphology. The tubular structures observed with confocal microscopy were directly comparable in size to the fibrillar P10 structures previously observed in electron micrographs of virus-infected cells (van Oers et al., 1994). The diameter of these structures, in cross-section, has been estimated at 1–2 μm in their mature, fully developed form.

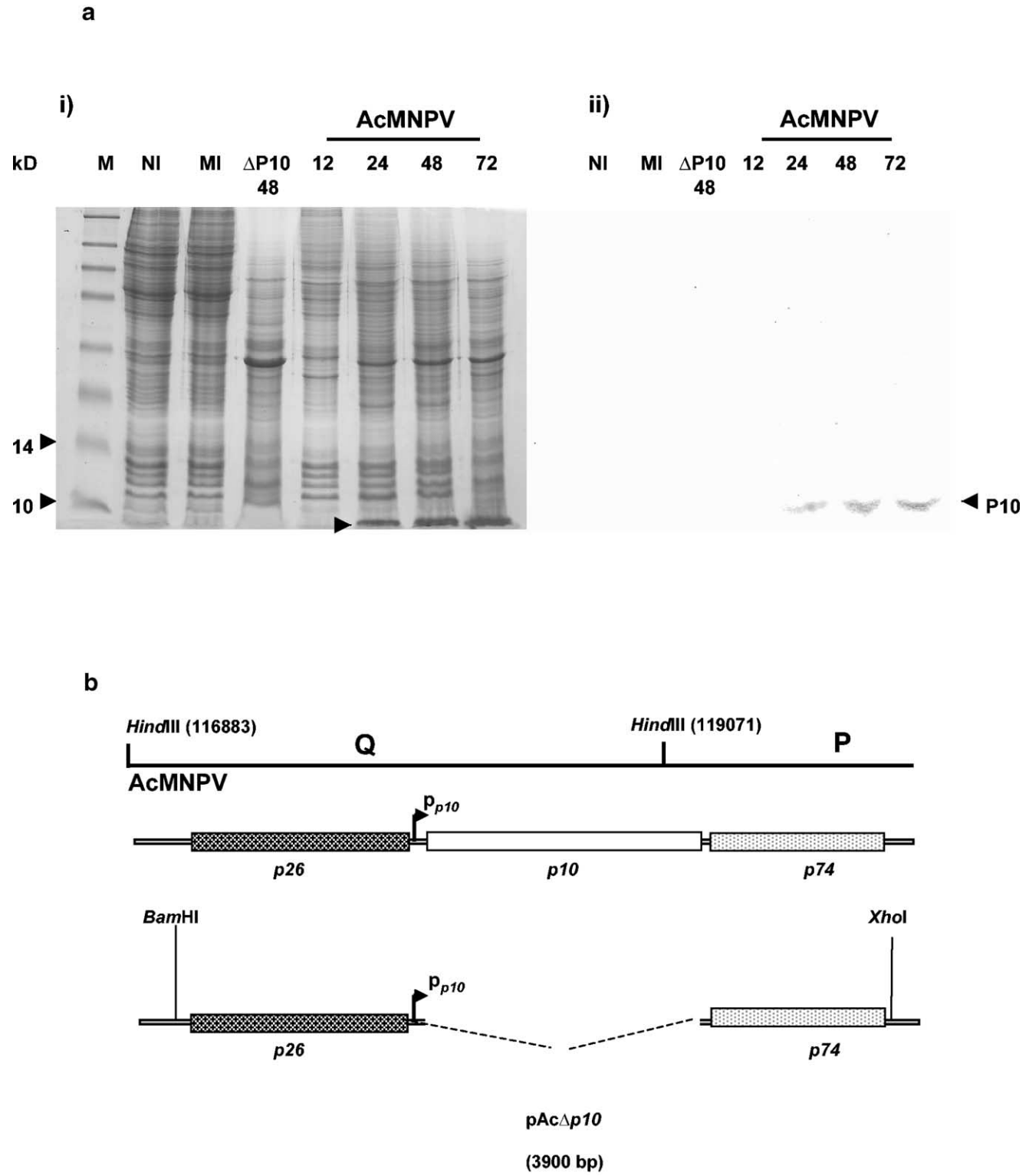

Fig. 1. (a)(i). Coomassie blue stained SDS–PAGE. Proteins from total cell extracts were analysed on 12% protein gels. Lanes: 1, Protein standards (New England Biolabs); 2, noninfected cells (NI); 3, mock-infected cells (MI); 4, AcΔ*p10*-infected cells at 48 hpi (Δ*p10*); 5–8, AcMNPV-infected cells at 12 (5), 24 (6), 48 (7), and 72 hpi (8). (ii) Western blot analysis of identical samples and gel loading order as in (i). The blot was probed with guinea pig P10 anti-peptide antiserum (1:500) and developed with Alkaline Phosphatase secondary serum. (b) Position of the *p10* gene on the AcMNPV genome. The gene spans the *Hin*dIII Q and P fragments of the AcMNPV genome. To create the AcΔ*p10* knockout virus, a transfer plasmid was designed, which encoded sequences identical to the upstream and downstream sequences flanking the *p10* coding region, without the *p10* gene. The flanking sequences were cloned between *Bam*HI and *Xho*I sites on a pBluescript vector.

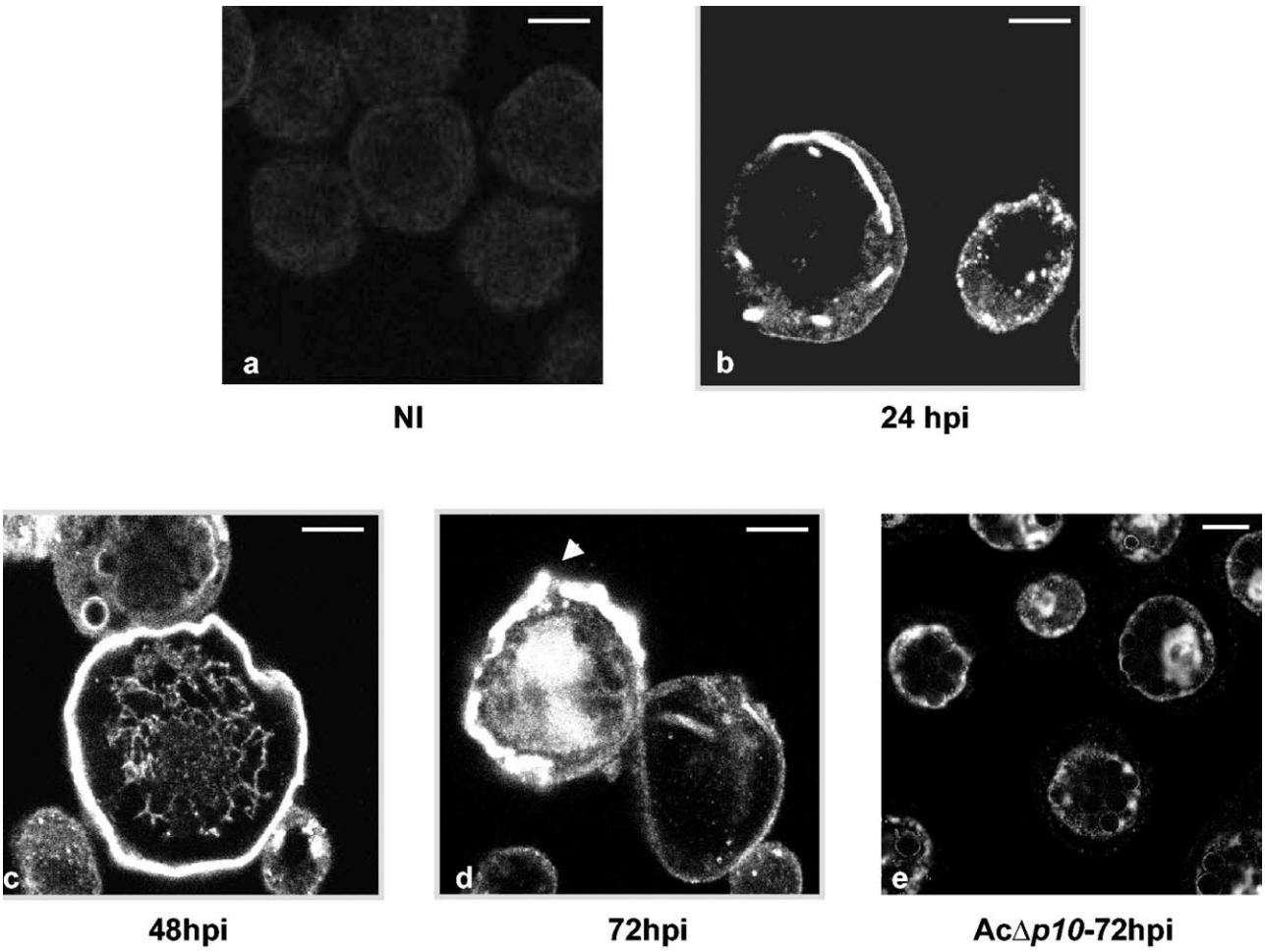

Fig. 2. Immunostaining of fixed Sf9 cells infected with AcMNPV. P10 was identified using a novel P10 antipeptide antiserum (1:250), and labelled with FITC-conjugated secondary antisera. (a) Noninfected Sf9 cells; (b) 24 hpi; (c) 48 hpi; (d) 72 hpi; and (e) AcΔ*p10*-infected cells, counterstained with propidium iodide. Disruption of the P10 sheath at 72 hpi (d) is arrowed. Scale bar: 5 μm.

Subcellular localisation of P10

AcMNPV-infected cells were stained for P10 and labelled with a FITC-conjugated secondary serum and counterstained with propidium iodide to determine the subcellular localisation of P10. In noninfected Sf9 cells, there was no P10 staining, and propidium iodide staining of the nuclear DNA revealed an intact nucleus (Fig. 4a). Staining of AcMNPV-infected cells suggested that the P10 tubular structures originated from the cytoplasmic side of the plasma membrane and extended to the cell's nucleus over time (24–72 hpi, Figs. 4b–d). The P10 structures were visible from 24 hpi (Fig. 4b). At this time point during infection, the P10 polymers were viewed largely in the cytoplasm, although some were detected in the nucleus. By 48 hpi (Fig. 4c), the P10 tubular structures intensified and became larger and were present in the nuclei, although they were still visible in the cytoplasm. During the final stages of infection (72 hpi; Fig. 4d), a thick sheath of P10 was observed underneath both the plasma membrane and the nuclear envelope, together with dense tubular structures in the nuclei of virus-infected cells.

P10. and F-actin

The well-defined distribution of P10 underneath the plasma and nuclear membranes suggested a close association with host cytoskeletal elements. To test this hypothesis, dual staining experiments were carried out to detect any relationship between P10 and host-cell cytoskeletal elements. Costaining of P10 together with F-actin was carried out in nonfixed, permeabilised cells, but did not suggest any obvious interaction between the two. The purpose for using nonfixed cells was to preserve F-actin, as fixation was shown to interfere with the preservation of actin filaments. The distribution of F-actin in noninfected cells was observed using Alexa 488 phalloidin, and propidium iodide counterstain outlined the area of the nucleus. The cells were stained with the P10 antiserum and probed with an anti-guinea pig Texas red secondary serum. In noninfected cells,

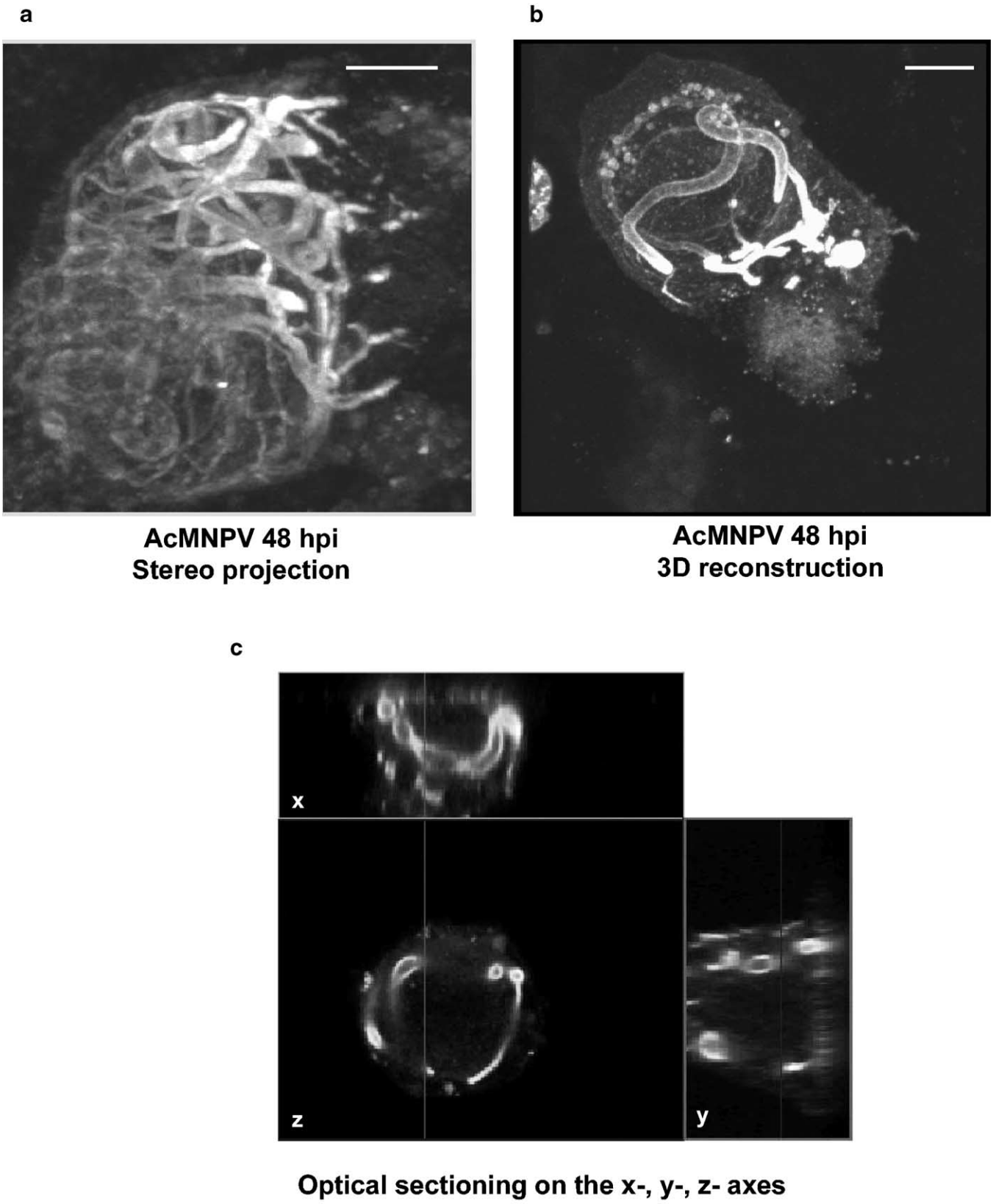

Fig. 3. P10 localisation in AcMNPV-infected Sf9 cells. (a) Stereo projection of a fixed AcMNPV-infected Sf9 cell, 48 hpi. (b) Three-dimensional reconstruction of a Sf9 cell infected with AcMNPV and fixed at 48 hpi. (c) Optical sectioning of an infected cell at 48 hpi and visualisation of the *x*, *y*, and *z* planes. In each image the cells were stained using the P10 antipeptide antiserum, as described in Fig. 2. Scale bar: 5 μm.

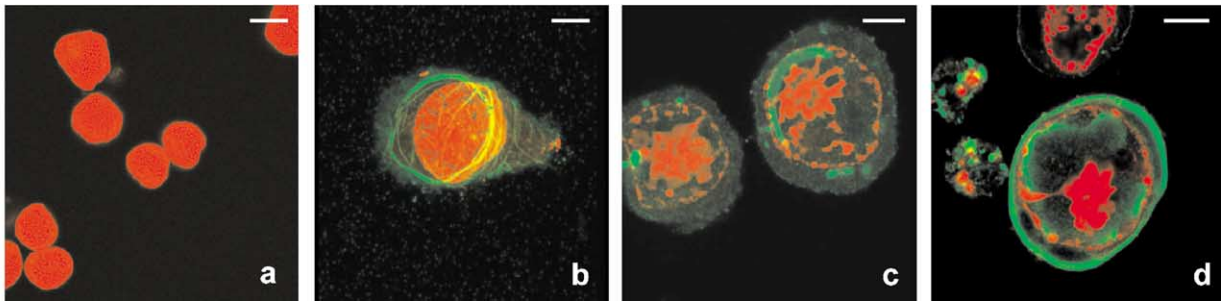

4

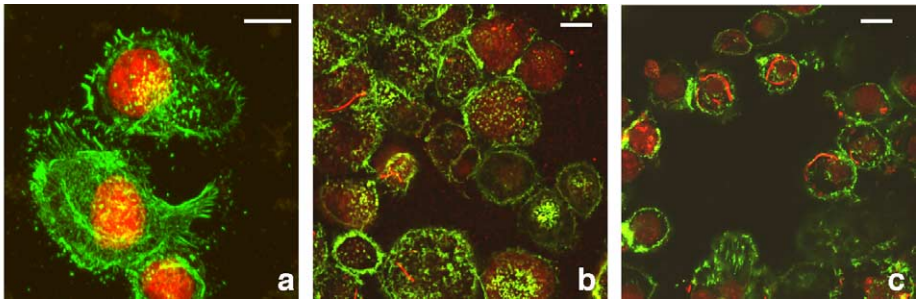

5

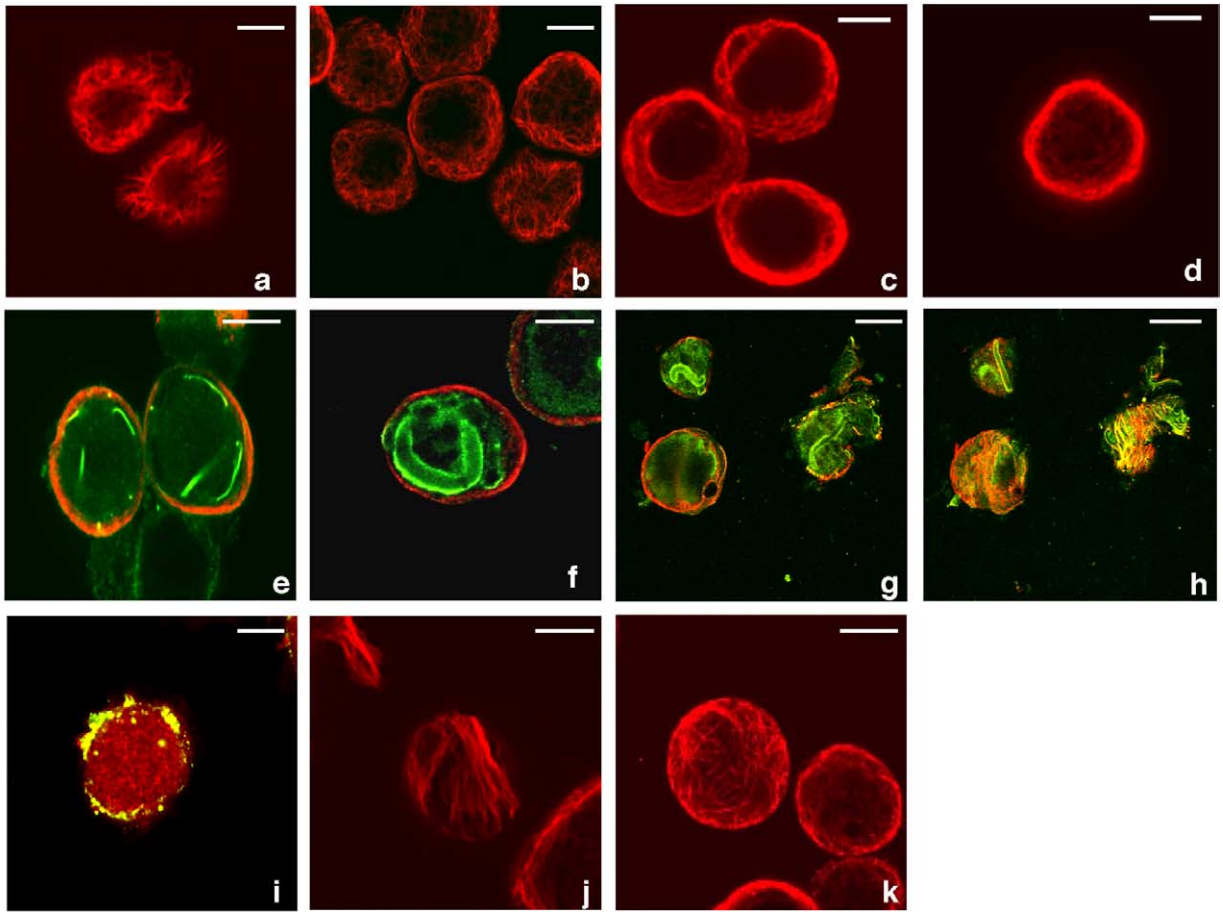

6

F-actin formed stress fibres and was associated with filipodian extensions (Fig. 5a). In virus-infected cells at 24 and 48 hpi (Figs. 5b and c, respectively), F-actin staining was punctuate in appearance and less abundant than in noninfected cells, but did not colocalise with the P10 tubular structures late in infection.

P10 and microtubules

Immunofluorescence studies on the P10 protein from OpMNPV showed that a monoclonal antiserum developed against P10 also recognised microtubules (Quant-Russell et al., 1987), suggesting that there may be an interaction between P10 and microtubules. The microtubules in noninfected Sf9 cells extended from the perinuclear region to the cytoplasmic periphery (Fig. 6a). In cells infected with wild-type AcMNPV, microtubules progressively retracted underneath the plasma membrane from early time points after infection (Fig. 6b), and formed bundles, which persisted until the final stages of infection (Figs. 6c–d; 48 and 72 hpi, respectively). In dual-labelling experiments, P10-antibody complexes were probed with a FITC-conjugated secondary serum, whereas α-tubulin was labelled with a Texas red anti-rat serum (Figs. 6e–g). A close relationship between P10 and α-tubulin was observed from as early as 18 hpi (data not shown). At 24 hpi, P10 cables were observed in the cytoplasm, close to cortical microtubules, which by this time in infection had retracted underneath the plasma membrane (Fig. 6e). During the later stages of infection (48 and 72 hpi; Figs. 6f–g, respectively), the P10 structures found in the cytoplasm were also in close proximity to cortical microtubules. At the very late stages of infection microtubule bundles were observed, and these were partly colocalising with the P10 tubular structures as indicated by the yellow colouration (Fig. 6h).

The relationship between P10 and α-tubulin was observed in cells treated with the microtubule-depolymerising agent nocodazole (Fig. 6i). The drug was titrated in S*f*9 cells and was found to be most effective at a concentration of 25 μM. This was the concentration that induced complete depolymerisation of microtubules within 4 h of treatment, and with the least cell mortality ($<$30%). A negative control of virus-infected cells treated with DMSO, the diluent of nocodazole, was also included (Fig. 6j). CLSM images of dual-labelled cells showed that in nocodazole-treated cells, the microtubules were depolymerised and there was no pattern in their cytoplasmic distribution. Patches of P10 could be detected in the cytoplasm of virus-infected cells, but no tubular structures were ever observed. Control of cells treated with DMSO, the diluent of nocodazole, did not show altered morphology of the microtubules, or the P10 tubular structures (data not shown). This provided evidence that polymerised microtubules were required for the formation of P10 tubules.

In Sf9 cells infected with the AcΔ*p10* virus, the distribution of the microtubules was different than the pattern observed in AcMNPV-infected cells. In cells infected with AcΔ*p10* virus, the microtubules did not form bundles at 72 hpi, as occurs during infection of the cells with AcMNPV (Fig. 6k), but formed arrays throughout the cytoplasm (Fig. 6l).

Protein–protein interactions using coimmunoprecipitations and yeast two-hybrid assays

Further to the CLSM evidence demonstrating an interaction between P10 and microtubules, immunoprecipitation experiments were carried out to detect protein–protein interactions between P10 and α-tubulin.

Total cellular protein from Sf9 cells infected with AcMNPV or the AcΔ*p10* virus was allowed to form immunocomplexes with either anti-P10 or anti-α-tubulin antibodies. These immunocomplexes were captured on columns and the retained antigens were washed thoroughly from nonspecific cell debris and proteins. The retained antigens were eluted from the columns and subjected to separation on SDS–polyacrylamide gels. The proteins were transferred onto nitrocellulose membranes and probed with either anti-P10 or anti-α-tubulin antibodies.

The immunocomplexes created using the P10-specific antibodies were shown to contain P10 and α-tubulin by immunobloting with the P10- (Fig. 7a) and tubulin-specific sera (Fig. 7b). Similarly, the anti-α-tubulin antiserum immunocomplexes were also analysed and tested positively for the presence of P10 (Fig. 7c) and α-tubulin (Fig. 7d).

The results of the immunoprecipitations suggested protein–protein interactions between P10 and α-tubulin and these findings were further supported by yeast two-hybrid analyses. The

Fig. 4. Immunofluorescence staining of AcMNPV-infected Sf9 cells. (a) Propidium iodide staining of noninfected cells (red). (b–d) AcMNPV-infected cells at (b) 24 hpi; (c) 48 hpi; and (d) 72 hpi. Cells were stained with propidium iodide for nuclear DNA (red) and P10 was identified with P10 antiserum and labelled with FITC-conjugated secondary serum (green). Scale bar: 5 μm.

Fig. 5. Co-staining for P10 and F-actin. (a) Noninfected Sf9 cells stained with Alexa 488 phalloidin for F-actin (green), and propidium iodide for nuclear DNA (red). (b–c) AcMNPV-infected cells at 24 hpi (b) and 48 hpi (c) probed for F-actin (green) and P10 (red). P10 was labelled with TRITC-conjugated secondary serum. Scale bar: 5 μm.

Fig. 6. Dual staining for microtubules (red) and P10 (green). (a) Microtubules in noninfected Sf9 cells; (b–d) microtubules in AcMNPV-infected Sf9 cells at 24 hpi (b), 48 hpi (c), and 72 hpi (d); (e–g) AcMNPV-infected cells at 24 hpi (e), 48 hpi (f), and 72 hpi (g) stained for P10 (green) and microtubules (red). Yellow-orange appears at the points of colocalisation; (h) Sf9 cells treated with nocodazole and stained for P10 (green) and microtubules (red). The points of colocalisation appear yellow; (i) ventral image of a virus-infected cell stained for P10 (green) and α-tubulin (red); (j) ventral image of an AcMNPV-infected cell at 72 hpi stained for α-tubulin (red), and (k) ventral image of an AcΔ*p10*-infected cell at 72 hpi stained for α-tubulin (red) and P10 (green). Scale bar: 5 μm.

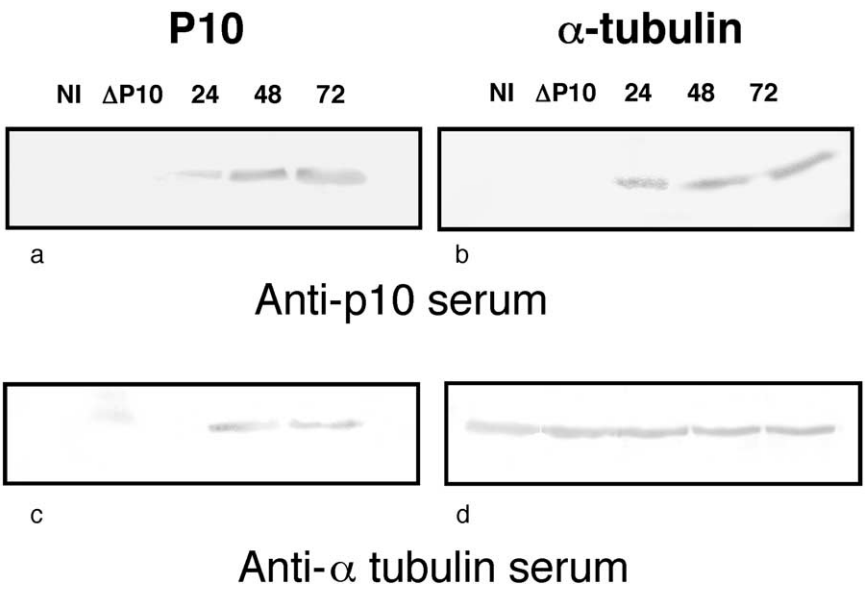

Fig. 7. Coimmunoprecipitation of P10 and α-tubulin. (a–b) Western blot analysis of immunoprecipitates formed using P10 antiserum in whole-cell extracts (a, blotted with the P10 antiserum; b, blotted with anti-α-tubulin antiserum). (c–d) Western blot analysis of immunoprecipitates formed using the α-tubulin antiserum (c, blotted with P10 antiserum; and d, with α-tubulin antiserum). Lanes: (1) noninfected cells (NI); (2) AcΔ*p10*-infected cells at 72 hpi (ΔP10); (3–5) AcMNPV-infected cells at 24 hpi (3), 48 hpi (4), and 72 hpi (5).

p10 gene from AcMNPV and a human α-tubulin gene were cloned in both pBridge and pGAD-T7 vectors. These vectors were used pairwise to transform competent *S. cerevisiae* AH109 cells. The transformants were allowed to grow on low-, medium-, and high-stringency media. Although some false positives occurred in colonies grown on low- and medium-stringency media, none were detected in high-stringency media (Table 1). The colonies for the paired pBridge/*p10* and pGAD-T7/*p10* (and vice versa), pBridge/*p10* and pGAD-T7/α-tubulin, and pBridge/α-tubulin and pGAD-T7/*p10* appeared blue. The presence of positive transformants on the high-stringency medium indicated that the interactions between P10 and P10 (used as positive control), but also between P10 and α-tubulin, were strong.

The putative microtubule-binding domain on P10

Further to the prediction by van Oers and Vlak (1997) for a putative microtubule-binding domain on the basic part of P10, the primary amino acid sequence of the AcMNPV P10 protein was analysed using algorithmic modules available on the worldwide web (www.expasy.ch). The carboxy-terminal amino acids of the protein had a theoretical isoelectric point at 9.31, demonstrating the alkaline profile of the C-terminus. Furthermore, the amino acid composition of the C-terminus revealed that, with the exception of valine, the content of the last 44 amino acids was significantly rich in lysine, proline, and glycine (Table 2), which is characteristic of "conventional" microtubule-associated proteins (Aizawa et al., 1989; Tokuraku et al., 1999).

Discussion

The present study reports on the involvement of host-cell microtubules in the formation of P10 tubular structures. This work benefited from the production of a very specific antiserum against an antigenic peptide, identical to the carboxy-terminus of the P10 protein from AcMNPV. Unlike other sera used in previous research that were reported to

Table 1
Pairwise transformations for yeast two-hybrid analyses

	Carrier DNA (Herring testes DNA)	pBridge vector only	pGAD-T7 vector only	pBridge/ α-tubulin	pBridge/*p10*
Carrier DNA (Herring testes DNA)	−	−	−	−	+
pBridge vector only	−	+	−	−	+
pGAD-T7 vector only	−	−	−	+	+
pGAD-T7/α-tubulin	−	−	+	+	+++
pGAD-T7/*p10*	−	−	+	++	+++

+, colonies on low stringency media; ++, colonies on medium stringency media; +++, colonies on high stringency media.

Table 2
Amino acid composition of conventional MAPs and P10s

Protein	Theoretical pl	Valine (%)	Lysine (%)	Proline (%)	Glycine (%)
Conventional MAPs	9–11	6–25	11–46	3–17	0–22
AcMNPV P10	9.31	2.3	13.6	6.8	4.6
SeMNPV P10	11	0	31	6	6
CfMNPV P10	9.86	9.68	9.68	12.90	6.45
CfGV P10	10.50	9.52	19.05	14.29	0

cross-react with other host- or virus-related proteins (Quant-Russel et al., 1987), this antiserum was specific for the P10 protein, which was most useful for immunostaining of P10 in virus-infected cells. In addition, to act as a negative control in all experiments, we produced a modified AcMNPV in which the entire *p10* coding region had been deleted. CLSM examination of AcMNPV-infected cells revealed that P10 formed fibrous-like structures extending from the cytoplasm to the nucleus. By 48 hpi a thick sheath of P10 was evident beneath the plasma membrane and at the very late stages this sheath was shown to fragment, concomitant with what appeared to be plasma membrane disruption and cellular lysis. Three-dimensional visualisations of fluorescently labelled P10 in AcMNPV-infected cells revealed that the protein appeared to polymerise to form tubular structures, which extended throughout the cell periphery. These structures were consistent with previously published electron micrographs of P10 in virus-infected cells (Williams et al., 1989; van Oers et al., 1994).

The definition of the P10 tubules suggested that a cytoskeletal element served as a scaffold. The distribution of F-actin and microtubules were examined carefully in virus-infected Sf9 cells. Staining for F-actin appeared punctuate but did not correlate with P10 staining. Using an antibody against α-tubulin, this component of the cytoskeleton was visualised initially in noninfected Sf9 cells and the pattern of distribution of the microtubules was observed to be very similar to that observed in mammalian cells, in which the microtubules originate from the perinuclear region and extend to the cellular periphery (Vorobjev et al., 1997). During the course of virus infection, the microtubules were observed to rearrange and form a lining underneath the plasma membrane, inducing rounding of infected cells in agreement with the results of Volkman and Zaal (1990). This lining persisted throughout the infection, as well as the bundles of cortical microtubules that formed as early as 24 hpi. This observation confirmed the results of Williams et al. (1989), who also described polymerised microtubules until the very late stages of infection.

Although the function of the P10 tubular structures was not obvious at this stage, it was clear that their formation was dependent on the presence of intact microtubules. This was further supported by treatment of virus-infected cells with the microtubule-disrupting agent nocodazole (Hollinshead et al., 2001; Blajeski et al., 2002). Prior to use with virus-infected cells, Nocodazole was titrated, and the concentration used in Sf9 cells (25 μM) was shown to depolymerise microtubules in approximately 4 h, and without high cell mortality rates. Observation of nocodazole-treated cells showed that the microtubules depolymerised completely, and the tubular structures of P10 disappeared, although P10 could still be detected in cytoplasmic pools. Similarly, bundling of microtubules during AcMNPV infection seemed to be dependent on the presence of P10. During infection with the AcΔ*p10* virus, microtubules were detected in the cytoplasm of infected cells; however, no bundling could be observed, nor a specific pattern for distribution of microtubules underneath the plasma membrane.

On the association of P10 with microtubules, it was demonstrated that MAP properties could be observed upon artificial phosphorylation of P10 (Cheley et al., 1992). We have shown with both visual and biochemical evidence that P10 does not require artificial phosphorylation to associate with microtubules. However, it is not known yet how P10 interacts with tubulin, and phosphorylation of the viral polypeptide by an intracellular, or even another virus-encoded protein, cannot be ruled out (Cheley et al., 1992), as phosphorylation is a predominant event for associations between conventional MAPs and microtubules. For example, the phosphorylated form of the microtubule-associated protein 1B (MAP 1B) is thought to bind microtubules more effectively than the nonphosphorylated form (Diaz-Nido et al., 1988; Goold et al., 1999).

Initial primary sequence analysis and motif prediction searches did not reveal any obvious microtubule-binding sequences on P10. More detailed analyses did show, however, that the last 44 amino acids of the carboxy-terminus give that region of P10 a basic profile, with a theoretical isoelectric point of 9.31. This is characteristic of microtubule-binding domains found on many MAPs, which exhibit isoelectric point values between 9 and 11 (Melki et al., 1991; Nguyen and Fasold, 1991). With the exception of valine, the carboxy-terminus of P10 is also enriched in the amino acids proline, lysine, and glycine, common to MAPs. This basic profile seems to be present in other P10 proteins encoded by both nucleopolyhedroviruses and granuloviruses (Table 2). In contrast, FALPE from the *Amsacta moorei* entomopoxvirus does not seem to have a basic domain. Generally, MAPs are believed to interact with MTs by means of an ionic interaction between their basic microtubule-binding domains and the acidic C-terminus of tubulin.

Site-directed mutagenesis is currently being employed to define and characterise the microtubule-binding site on P10. In addition the interactions between P10 and other host- and virus-encoded proteins are being examined. Taking into consideration that other microtubule-associated proteins are large molecules ranging between 48.5 kDa, e.g., the full-length Tau protein (Goedert and Jakes, 1990), and approximately 350 kDa, e.g., MAP 1A (Cravchik et al., 1994), then the small P10 is a unique molecule and may represent a novel group of virus-encoded MAPs.

Materials and methods

Cell line and viruses

The *Spodoptera frugiperda* (fall armyworm) Sf9 cell line was grown at 28°C in SF90011 serum-free medium (Invitrogen Ltd., UK). Passage 3 AcMNPV Clone 6 virus was propagated and amplified to high titre inoculum (1×10^8 PFU/ml) using standard methods (King and Possee, 1992). A modified AcMNPV virus, which lacked the whole p10 coding region, was also used. The p10-knockout virus, designated AcΔ*p10*, was produced by cotransfecting insect cells with linear virus DNA from AcUW1 (Weyer et al., 1990) and a transfer vector that included PCR-amplified ORFs (p26 and p74, respectively) flanking *p10*. The primers p26-Forward-*Bam*HI (GCG **GGA TCC** GCA TTG GAG CTC CAA TTT TTG CCG GC) and p26-Reverse (CAA TTG ATT TGT TAT TTT AAA AAC GAT TCA TGA TTG TAA ATA AAA TGA TAT TTA CAG TAT AG), and p74-Forward (T CAT GAA TCG TTT TTA AAA TAA CAA ATC AAT TG(CTA TAC TGT AAA TAT CAT TTT ATT TAC AA) and p74-Reverse-*Xho*I (GCG **CTC GAG** CGG AAA TGG TCG AAA CGG TCG ATG AC) were used to amplify 450 bp regions of the ORFs flanking the *p10* coding region. The restriction enzyme recognition sites are highlighted with bold characters and underlined. The two PCR products were used as template DNA in a second round of amplification to fuse the two flanking sequences by cross-over PCR using the primers p26-Forward-*Bam*HI and p74-Reverse-*Xho*I. The resulting product of the second amplification was inserted into pBC-SK(+) between the unique *Bam*HI and *Xho*I sites on the plasmid to produce the vector pAcΔ*p10* (as detailed in Fig. 1). AcΔ*p10* was amplified to high titre stocks (1×10^8 PFU/ml) and was propagated as described above.

Chemicals

Nocodazole (CN Biosciences, UK, Cat. No. 487928), supplied as 10 mg aliquots, was dissolved in 1 ml dimethyl sulphoxide (DMSO, Sigma-Aldrich, USA). The drug was titrated in noninfected Sf9 cells and the working concentration was determined as the amount of drug required to depolymerise microtubules in 4 h and with mortality <30%. 3-Maleimidobenzoic acid *N*-hydroxysuccinimide ester (MBS, Sigma-Aldrich) was dissolved in distilled water to produce a stock of 10 mM.

Antibodies

A rat polyclonal serum to α-tubulin (Cat. No. MCA77G) was purchased from Serotec (UK) and was used at a dilution of 1:150 in PBS–2% BSA for immunostaining, or 1:300 in PBST/5% dried milk for Western blot analyses. For immunoprecipitations, 100 μg of antibody was used for antibody–antigen complexes.

A specific peptide was produced identical to the last 16 amino acids at the carboxy-terminus of P10 from AcMNPV. The sequence was NH2-CFELDSDARRGKRSSK-COOH and was synthesised and HPLC-purified at the Centre for Proteins and Peptides, Oxford Brookes University. The purified peptide was used to immunise guinea pigs. Sera from the first and second booster were analysed for specificity to P10. The serum was used for immunostaining of cells at a dilution of 1:250 in PBS–2% BSA and 1:500 in Western blot analyses.

Western blot analysis

Twenty-milliliter shaker cultures of Sf9 cells at a density of 2×10^6 were infected with AcMNPV C6 at a multiplicity of 10 PFU/cell. Two-milliliter samples were collected at 12, 24, 48, and 72 hpi. The cells were pelleted by centrifugation and washed twice with sterile PBS before being resuspended in 80 μl PBS and 20 μl 6× denaturing protein gel loading buffer. The supernatants were treated with Strataclean resin (Stratagene Ltd., USA) for collection of proteins from the culture media. Proteins from both these fractions were separated on 0.1% sodium dodecyl sulphate (SDS)–15% polyacrylamide gels and transferred onto nitrocellulose membranes (Sambrook et al., 1982). The membranes were blocked in PBST buffer (PBS–0.1% Tween 20) containing 5% dried milk and probed with either anti-P10 serum (1:500) or anti-α-tubulin serum (1:300). Anti-guinea pig alkaline phosphatase conjugate secondary serum (Sigma-Aldrich, USA) was used for the P10 blots (1:10,000) and anti-rat alkaline phosphatase conjugate serum (1:10,000) (Sigma-Aldrich, USA) was used for the tubulin blots. The blots were developed using NBT (nitro blue tetrazolium, Cat. No. N6639, Sigma-Aldrich, UK) and BCIP (5-bromo-4-chloro-3-indoyl phosphate, Cat. No. B6149, Sigma-Aldrich, UK) (Sambrook et al., 1982).

Immunoprecipitations

Immunoprecipitations were carried out using the Seize × Protein A Immunoprecipitation Kit (Cat. No. 45215, Pierce Chemical Co., USA). In brief, 20-ml cultures of Sf9 cells (2×10^6 cells/ml) were infected with either AcMNPV C6 or AcΔ*p10* virus at a multiplicity of 10 PFU/cell. The cells

were harvested at 24, 48, and 72 hpi by centrifugation and lysed using buffer NTEP (50 mM Tris–HCl, pH 7.9, 150 mM NaCl; 5 mM EDTA, 0.5% v/v Nonidet P-40) as described by King and Possee (1992). Resin slurry (0.4 ml) containing Protein A agarose (ImmunoPure Plus Immobilised Protein A) was equilibrated and washed according to kit instructions. The required antibody (100 μg) was immobilised on the resin, using the cross-linking agent disuccinimidyl suberate (DSS) included in the kit. The protein extracts were added onto the antibody-containing columns and were incubated at 4°C with overnight rotating. The mixes were then sedimented in the column and crude material was washed away with the Quenching buffer provided. The remaining antigen was dissociated from the antibody, using the provided elution buffer (ImmunoPure Elution buffer). The elution process was repeated three more times and the fractions were examined by SDS–PAGE and Western blot analysis.

Yeast two-hybrid analyses

Protein–protein interactions were assayed using the MATCHMAKER Two-Hybrid System 3 (Becton–Dickinson Clontech, Ltd., USA). The *p10* coding sequence was cloned into pBridge, which contained the GAL4-binding domain (BD), and pGAD-T7 that encoded the GAL4-activation domain (AD). Similarly, a human α-tubulin gene (GenBank Accession No. AF081484) was cloned into the same vectors.

Freshly grown AH109 yeast was made competent using the lithium acetate method (Schiestl and Gietz, 1989; Hill et al., 1991; Gietz et al., 1992). The yeast was transformed with Herring testes carrier DNA (Sigma-Aldrich, UK) or plasmids only, to provide negative controls. Pairwise transformations of the plasmids containing the α-tubulin or the *p10* genes were carried out together with carrier DNA to determine protein–protein interactions. The transformants were plated out on low- (Synthetic Dropout (SD), -Leu, -Trp), medium- (SD, -His, -Leu, -Trp), and high- (SD, -Ade, -His, -Leu, -Trp, X-Gal) stringency media. Protein–protein interactions were determined by growth of yeast colonies on these media. To confirm the presence of both genes in these colonies, total DNA was extracted from yeast by boiling cells at 100°C for 15 min and used as template in PCR reactions together with the specific primers for *p10* and α-tubulin.

Immunofluorescence staining

Sterile coverslips (13 mm, No 0, Agar Scientific, medium) were seeded in the dishes (1×10^6 cells/dish) and left to attach. The culture media were removed and the cells were infected with AcMNPV, or AcΔ*p10* virus inoculum (10 PFU/cell). Following incubation at 28°C, cells at 24, 48, and 72 hpi were treated with 100 μg/ml RNAse A for 30 min at 37°C and subsequently fixed with 4% paraformaldehyde in 0.1 M PIPES, pH 6.9, 0.010 M EGTA, 0.010 M $MgCl_2$ (PEM) buffer for 45 min, before being permeabilised with 0.01% Triton X-100 in PBS/2% BSA (10 min, at room temperature). The staining procedure was carried out as described previously (Thomas et al., 1998). A final incubation with 3 μg/ml propidium jodide for 2 min was necessary for staining of nuclear DNA.

For visualisation of F-actin, noninfected and AcMNPV-infected cells were treated with 0.01 M MBS in PEM buffer, containing 0.1% Triton X-100. As preliminary studies had indicated that fixation did not produce consistent results for F-actin staining (data not shown), all the studies for F-actin were carried out in nonfixed cells (Collings et al., 2001). Immunostaining for P10 was carried out using the method described earlier and F-actin was stained with Alexa 488-conjugated phalloidin (Molecular Probes, USA).

Confocal microscopy

All immunostained samples were examined using a Zeiss 510 Confocal laser scanning microscope (LSM). Data acquisition was carried out using $\times$100 immersion oil lens, with a numerical aperture of 1.25 and an optical zoom of 2. Detection of green (FITC) and red (Texas red) fluorochromes was achieved using narrow band filter sets and three laser lines: argon 488 nm, and helium/neon 543 and 633 nm. Data were collected using the multi tracking facility on the microscope to avoid cross-talk. For three-dimensional reconstructions and stereo projections, optical sectioning of 200 nm (section thickness) was carried out using Zeiss software. This consisted of pictures of parallel planes through the cell, 310 nm apart from each other (a typical Z-stack of reconstructed Sf9 cells was approximately 20 μm in depth and included 63 images). All measurements, including cell-depth calculations and scale bars, were calculated using the Zeiss LSM 510 software.

Image processing

Confocal microscopic images were exported to Windows directories as TIFF (Tagged Image Format File) files from the Zeiss 510 Image Browser. These images were converted into JPEG (Joint Photographic Experts Group) files in Adobe Photoshop 6.0. Serial images were also converted into JPEG files before imported into Adobe Premiere 6.0 to be compiled into AVI (Audio Video Interleave) animation files, at a speed of three frames per second.

Acknowledgments

We thank Professor Chris Hawes and Jan Evins for help and advice on microscopy and Professor Nigel Groome and Dr. Carole Thomas for advice and help in preparing the P10 antiserum. We also thank Dr. Joanne Maitland and Dr. Simon Dawson, University of Nottingham, for providing

the strains for the yeast two-hybrid system and helpful comments. This work was partially funded by the BBSRC Bioimaging initiative and the Natural Environmental Research Council.

References

Adang, M.J., Miller, L.K., 1982. Molecular cloning of DNA complementary to messenger RNA of the baculovirus *Autographa californica* nuclear polyhedrosis virus location and gene products of RNA transcripts found late in infection. J. Virol. 44, 782–793.

Aizawa, H., Kawasaki, H., Murofushi, H., Kotani, S., Suzuki, K., Sakai, H., 1989. A common amino acid sequence in 190-kDa microtubule-associated protein and tau for the promotion of microtubule assembly. J. Biol. Chem. 264, 5885–5890.

Alaoui-Ismaili, M.H., Richardson, C.D., 1996. Identification and characterization of a filament-associated protein encoded by *Amsacta moorei* entomopoxvirus. J. Virol. 70, 2697–2705.

Allen, T.D., Cronshaw, J.M., Bagley, S., Kiseleva, E., Goldberg, M.W., 2000. The nuclear pore complex: mediator of translocation between nucleus and cytoplasm. J. Cell Sci. 113, 1651–1659.

Ayres, M.D., Howard, S.C., Kuzio, J., Lopez-Ferber, M., Possee, R.D., 1994. The complete DNA sequence of *Autographa californica* nuclear polyhedrosis virus. Virology 202, 586–605.

Blajeski, A.L., Phan, V.A., Kottke, T.J., Kaufmann, S.H., 2002. G(1) and G(2) cell-cycle arrest following microtubule depolymerization in human breast cancer cells. J. Clin. Invest. 110, 91–99.

Cha, H.J., Dalal, N.G., Pham, M.Q., Kramer, S.F., Vakharia, V.N., Bentley, W.E., 2002. Monitoring foreign protein expression under baculovirus *p10* and *polh* promoters in insect larvae. Biotechniques 32, 986–988 990.

Cheley, S., Kosik, K.S., Paskevich, P., Bakalis, S., Bayley, H., 1992. Phosphorylated baculovirus p10 is a heat-stable microtubule-associated protein associated with process formation in Sf9 cells. J. Cell Sci. 102, 739–752.

Collings, D.A., Zsuppan, G., Allen, N.S., Blancaflor, E.B., 2001. Demonstration of prominent actin filaments in the root columella. Planta Med. 212, 392–403.

Cravchik, A., Reddy, D., Matus, A., 1994. Identification of a novel microtubule-binding domain in microtubule-associated protein 1A (MAP 1A). J. Cell Sci. 107, 661–672.

Croizier, G., Gonnet, P., Devauchelle, G., 1987. Localisation cytologique de la proteine non structurale p10 du baculovirus de la polyhedrose nucleaire du Lepidoptere *Galleria mellonella* L. C.R. Acad. Sci. Serie III (Paris) 305, 677–681.

Diaz-Nido, J., Serrano, L., Mendez, E., Avila, J., 1988. A casein kinase II-related activity is involved in phosphorylation of microtubule-associated protein MAP 1B during neuroblastoma cell differentiation. J. Cell. Biol. 106, 2057–2065.

Eldridge, R., Li, Y., Miller, L.K., 1992. Characterisation of a baculovirus gene encoding a small conotoxin-like peptide. J. Virol. 66, 6563–6571.

Facanha, A.L., Appelgren, H., Tabish, M., Okorokov, L., Ekwall, K., 2002. The endoplasmic reticulum cation P-type ATPase Cta4p is required for control of cell shape and microtubule dynamics. J. Cell. Biol. 157, 1029–1039.

Feldher, C.M., Atkin, D., 1997. The location of the transport gate in the nuclear pore complex. J. Cell Sci. 110, 3065–3070.

Fielding, B.C., Davison, S., 2000. Identification and characterization of the *Trichoplusia ni* single capsid nuclear polyhedrosis virus *p10* gene. Virus Genes. 20, 189–192.

Gietz, D., St. Jean, A., Woods, R.A., Schiestl, R.H., 1992. Improved method for high efficiency transformation of intact yeast cells. Nucleic Acids Res. 20, 1425.

Goedert, M., Jakes, R., 1990. Expression of separate isoforms of human tau protein: correlation with the tau pattern in brain and effects on tubulin polymerization. EMBO J. 13, 4225–4230.

Goold, R.G., Owen, R., Gordon-Weeks, P.R., 1999. Glycogen synthase kinase 3β phosphorylation of microtubule-associated protein 1B regulates the stability of microtubules in growth cones. J. Cell Sci. 192, 3373–3384.

Hayat, M.A., 2000. Principles and Techniques of Electron Microscopy (Biological Applications), Fourth ed. Cambridge Univ. Press, Cambridge, UK.

Hill, J., Donald, K.A., Griffiths, D.E., Donald, G., 1991. DMSO-enhanced whole cell yeast transformation. Nucleic Acids Res. 19, 5791.

Hollinshead, M., Rodger, G., Van Eijl, H., Law, M., Hollinshead, R., Vaux, D.J.T., Smith, G.L., 2001. Vaccinia virus utilizes microtubules for movement to the cell surface. J. Cell. Biol. 154, 389–402.

Hooft van Iddekinnge, B.J.L., Smith, G.E., Summers, M.D., 1983. Nucleotide sequence of the polyhedrin gene of *Autographa californica* nuclear polyhedrosis virus. Virology 131, 561.

Jarvis, D.L., Bohlmeyer, D.A., Garcia Jr., A., 1991. Requirements for nuclear localization and supramolecular assembly of a baculovirus polyhedrin protein. Virology 185, 795–810.

Kallio, M.J., Beardmore, V.A., Weinstein, J., Gorbsky, G.J., 2002. Rapid microtubule-independent dynamics of Cdc20 at kinetochores and centrosomes in mammalian cells. J. Cell Biol. 158, 841–847.

King, L.A., Possee, R.D., 1992. The Baculovirus Expression System: A Laboratory Guide. Chapman and Hall, London.

Krappa, R., Knebel-Morsdorf, D., 1991. Identification of the very early transcribed baculovirus gene PE-38. J. Virol. 65, 805–812.

Kuzio, J., Rohel, D.Z., Curry, C.J., Krebs, A., Carstens, E.B., Faulkner, P., 1984. Nucleotide sequence of the p10 polypeptide gene of *Autographa californica* nuclear polyhedrosis virus. Virology. 139, 414.

Lagunoff, D., Chi, E.Y., 1976. Effect of colchicine on rat mast cells. J. Cell. Biol. 71, 182–195.

McGill, M., Brinkley, B.R., 1975. Human chromosomes and centrioles as nucleating sites for the in vitro assembly of microtubules from bovine brain tubulin. J. Cell. Biol. 67, 189–199.

Melki, R., Kerjan, P., Waller, J.P., Carlier, M.F., Pantaloni, D., 1991. Interaction of microtubule-associated proteins with microtubules: yeast lysyl- and valyl-tRNA synthetases and tau 218–235 synthetic peptide as model systems. Biochemistry 10, 11536–11545.

Morris, T.D., Miller, L.K., 1994. Mutational analysis of a baculovirus major late promoter. Gene 140, 147.

Nguyen, M., Fasold, H., 1991. A strongly basic protein of the MAP2 family copolymerizes with tubulin and induces polymerization. J. Protein Chem. 10, 511–516.

Possee, R.D., Howard, S., 1987. Analysis of the polyhedrin gene promoter of the *Autographa californica* nuclear polyhedrosis virus. Nucleic Acids Res. 15, 10233.

Quant-Russell, R.L., Pearson, M.N., Rohrmann, G.F., Beaudreau, G.S., 1987. Characterisation of baculovirus p10 synthesis using monoclonal antibodies. Virology 160, 9–19.

Razuck, F.B., Ribeiro, B., Vargas, J.H., Wolff, J.L., Ribeiro, B.M., 2002. Characterization of the p10 gene region of *Anticarsia gemmatalis* nucleopolyhedrovirus. Virus Genes 24, 243–247.

Rohel, D.Z., Cochran, M.A., Faulkner, P., 1983. Characterisation of two abundant mRNAs of *Autographa californica* nuclear polyhedrosis virus present late in infection. Virology 124, 357–365.

Sambrook, J., Fritch, E.F., Maniatis, T., 1982. Molecular Cloning: A Laboratory Manual, second ed. Cold Spring Harbor Laboratory Press, Cold Spring Harbor, NY.

Schiestl, R.H., Gietz, R.D., 1989. High efficiency transformation of intact yeast cells using single stranded nucleic acids as a carrier. Curr. Genet. 5-6, 339–346.

Sluder, G., 1979. Role of spindle microtubules in the control of cell cycle timing. J. Cell. Biol. 80, 674–691.

Smith, G.E., Vlak, J.M., Summers, M.D., 1983. Physical analysis of *Autographa californica* nuclear polyhedrosis virus transcripts for polyhedrin and 10,000-molecular-weight protein. J. Virol. 45, 215–225.

Thielmann, D.A., Stewart, S., 1991. Identification and characterisation of the *IE-1* gene of *Orgyia pseudotsugata* multicapsid nuclear polyhedrosis virus. Virology 180, 492–508.

Thomas, C.J., Brown, H.L., Hawes, C.R., Lee, B.Y., Min, M.K., King, L.A., Possee, R.D., 1998. Localisation of a baculovirus-induced chitinase in the insect cell endoplasmic reticulum. J. Virol. 72, 10207–10212.

Tokuraku, K., Katsuki, M., Matui, T., Kuroya, T., Kotani, S., 1999. Microtubule-binding property of microtubule-associated protein 2 differs from that of microtubule-associated protein 4 and tau. Eur. J. Biochem. 264, 996–1001.

van der Wilk, F., van Lent, J.W.M., Vlak, J.M., 1987. Immunogold detection of polyhedrin, p10 and virion antigens in *Autographa californica* nuclear polyhedrosis virus. Arch. Virol. 111, 103.

van Lier, F.L., van Duijnhoven, G.C., de Vaan, M.M., Vlak, J.M., Tramper, J., 1994. Continuous beta-galactosidase production in insect cells with a p10 gene based baculovirus vector in a two-stage bioreactor system. Biotech. Progr. 10, 60.

van Oers, M.M., Flipse, J.T., Reusken, E.L., Vlak, J.M., 1994. Specificity of baculovirus p10 functions. Virology 200, 513–523.

van Oers, M.M., Vlak, J.M., 1997. The baculovirus 10kDa protein. J. Invertebr. Pathol. 70, 1–17.

van Oers, M.M., Vlak, J.M., Voorma, H.O., Thomas, A.A., 1999. Role of the 3′ untranslated region of baculovirus p10 mRNA in high-level expression of foreign genes. J. Gen. Virol. 80, 2253–2262.

Vlak, J.M., Smith, G.E., Summers, M.D., 1981. Hybridisation, selection and *in vitro* translation of *Autographa californica* nuclear polyhedrosis virus mRNA. J. Virol. 40, 762–771.

Volkman, LE, Zaal, K.J., 1990. *Autographa californica* M nuclear polyhedrosis virus: microtubules and replication. Virology 175, 292–302.

Vorobjev, I.A., Svitkina, T.M., Borisy, G.G., 1997. Cytoplasmic assembly of microtubules in cultured cells. J. Cell Sci. 110, 2635–2645.

Wagner, U., Utton, M., Gallo, J.M., Miller, C.C.J., 1996. Cellular phosphorylation of tau by GSK-3β influences tau binding to microtubules and microtubule organization. J. Cell Sci. 109, 1537–1543.

Weyer, U., Knight, S., Possee, R.D., 1990. Analysis of very late gene expression by *Autographa californica* nuclear polyhedrosis virus and the further development of multiple expression vectors. J. Gen. Virol. 71 (7), 1525–1534.

Williams, G.V., Rohel, D.Z., Kuzio, J., Faulkner, P., 1989. A cytopathological investigation of *Autographa californica* nuclear polyhedrosis virus p10 gene function using insertion/deletion mutants. J. Gen. Virol. 70, 187–202.

Wilson, J.A., Hill, J.E., Kuzio, J., Faulkner, P., 1995. Sequence and transcriptional analysis of the baculovirus *Choristoneura fumiferana* multicapsid nuclear polyhedrosis virus (CfMNPV) p10 gene: identification of a coiled coil domain. J. Gen. Virol. 76, 2923–2932.

Zhang, F., Murhammer, D.W., Linhardt, R.J., 2002. Enzyme kinetics and glycan structural characterization of secreted alkaline phosphatase prepared using the baculovirus expression vector system. Appl. Biochem. Biotechnol. 101, 197–210.

Zhou, J., Yao, J., Joshi, H.C., 2002. Attachment and tension in the spindle assembly checkpoint. J. Cell Sci. 115, 3547–3555.

Zuidema, D., van Oers, M.M., van Strien, E.A., Caballero, P.C., Klok, E.-J., Goldbach, R.W., Vlak, J.M., 1993. Nucleotide sequence and transcriptional analysis of the p10 gene of *Spodoptera exigua* nuclear polyhedrosis virus. J. Gen. Virol. 74, 1017–1024.